Engineering Chemistry
ISSN: 2813-6535, Vol. 11, pp 39-52
doi:10.4028/p-QWZ5u3

Submitted: 2025-05-01
Revised: 2025-07-12
Accepted: 2025-07-25
Online: 2025-09-10

Application of the Swan Model for the Adsorption of Ni^{2+} and Cd^{2+} on Chitosan Derivative in a Packed Bed Column

I.G. Mkhize[1,a], E. Igberase[2,b*]

[1,2]Durban University of Technology, Department of Chemical Engineering, Steve Biko Campus, Durban, South Africa

Email: [a]innocentiaM2@dut.ac.za, [*]Email: [b]ephraimi@dut.ac.za

Keywords: Simulation; Regeneration; Sustainable adsorbent; Adsorption kinetics, GCCHI beads, chitosan-chitin adsorbent, heavy metal removal, breakthrough analysis, Swan model.

Abstract. Water pollution by heavy metals constitutes a significant environmental and health risk, necessitating efficient and reusable adsorbents. The current study investigates the application of inexpensive biopolymer chitosan to extract Ni^{2+} and Cd^{2+} ions from aqueous solutions. Material characterization using X-ray diffraction (XRD) showed the amorphous nature (absence of peak at 10°), and Brunauer-Emmett-Teller (BET) analysis exhibited the mesoporous surface area of 302.12 m^2/g, suitable for the adsorption of metal ions. The Swan model was parameterized with batch-derived adsorption parameters (i.e., Q_{max} = 220 mg/g for Ni^{2+}, 226 mg/g for Cd^{2+}) and successfully predicted packed-bed breakthrough curves at optimum pH (7 for Ni^{2+}, 6 for Cd^{2+}), with transport rates of 3.65×10^{-11} m^2/s (Ni^{2+}) and 3.14×10^{-11} m^{2+}/s (Cd^{2+}) for a 1.2 m column. The material retained over 95% removal efficiency after five regeneration cycles. These findings show the potential of chitosan for large-scale water treatment with high efficiency, model-driven design, and strong reusability.

Introduction

Heavy metal pollution remains one of our most pressing environmental challenges, with cadmium (Cd^{2+}) and nickel (Ni^{2+}) representing persistent and toxic threats to ecosystems and human health. These hazardous metals are primarily discharged from industrial processes like metal plating, mining, and steel production [1,2]. They bioaccumulate in living organisms and, according to the United States Environmental Protection Agency (USEPA), can cause serious health issues such as cancer and organ damage [3]. Chitosan has attracted interest as a biosorbent due to its biocompatibility and metal-binding properties. However, its real-world use is limited by poor acid stability, low adsorption capacity, and inadequate selectivity in mixed-metal environments.

In this study, grafted-cross-linked chitosan (GCCHI) beads were developed as an innovative adsorbent material that offers enhanced performance for real-world water treatment applications. The research establishes three key advances: firstly, the authors demonstrated how strategic material modification through cross-linking with chloromethyl oxirane and subsequent grafting with polydopamine improves acid stability, adsorption capacity, and selectivity for target metals. Secondly, the authors provided the first comprehensive evaluation of chitosan-based adsorbents for competitive Cd^{2+} and Ni^{2+} removal under environmentally relevant conditions, filling a crucial gap in existing literature that predominantly focuses on single-metal systems. Thirdly, the Swan model was implemented as a predictive tool for column kinetics, enabling more accurate scaling from laboratory experiments to potential industrial applications.

The novelty of this work lies in its integrated approach that combines material science innovation with practical engineering considerations. Unlike previous studies that examined adsorption performance in isolation [4] This study systematically evaluates both the fundamental adsorption mechanisms and the operational parameters critical for real-world implementation. The GCCHI beads developed here exhibit exceptional regeneration capability, maintaining over 95% of their initial adsorption capacity through multiple cycles. They significantly improve over conventional chitosan

adsorbents that typically show rapid performance degradation. Furthermore, the successful application of the Swan model provides a valuable tool for process optimization, addressing a longstanding challenge in translating batch adsorption results to continuous flow systems. Unlike conventional models like Thomas or Yoon-Nelson, the Swan model was utilized because it can predict column behavior directly from batch-derived parameters without further calibration. Its mechanistic description particularly includes film diffusion and intraparticle diffusion resistances, essential in properly simulating transport in porous chitosan-based adsorbents [5]. The model operates with zero initial concentration and constant inlet concentration boundary conditions. Established for chitosan systems to within 5% error in breakthrough curve predictions, the Swan model has variable process conditions like 2-10 BV/h flow rates and bed heights of 0.5-2 m. With this combination of features, scaling from laboratory to plant scale can be done more accurately, and information regarding rate-limiting adsorption mechanisms can also be obtained. The established efficacy of the model using biopolymer adsorbents and its ability to bridge batch and continuous-flow systems make it particularly appealing to evaluate the effectiveness of GCCHI beads for use in water treatment processes. This work advances our understanding of chitosan-based metal adsorption by bridging the gap between material development and process engineering. It provides a practical framework for developing more effective water treatment technologies. The findings offer tangible solutions to current limitations in heavy metal remediation while establishing methodologies that can be extended to other challenging wastewater contaminants.

Experimental

Adsorbent production process

Chitosan powder was purchased from Fengchen Group, China, while chloromethyl oxirane, acetic acid, sodium hydroxide, and polydopamine were purchased from Sigma-Aldrich, South Africa. The conversion to grafted chitosan composites (GCCHI) involves a dissolution of 30 grams of chitosan powder in a 10 percent acetic acid solution of one liter. For the cross-linking reaction, a 2.5% solution of chloromethyl oxirane is added and thoroughly stirred for 2 hours. The formed solution is pumped to a bath of 1M sodium hydroxide, where precipitation of solid CCHI beads occurs. To accomplish the grafting step, 5 g of such beads are mixed with 0.5g/L polydopamine solution in the open-neck flask. The mixture is irradiated using high-power microwaves at medium-low power. Polydopamine is used as a flexible cross-linker that can improve the adhesion abilities of the beads, and this is done within a 20-minute process. The last step makes it possible to functionalize the chitosan composite material further.

Characterization of adsorbent

The Shimadzu XRD model 7000 was used to capture diffraction patterns, which were obtained using a Bruker D8 Advance diffractometer (Germany) using Cu Kα radiation (λ = 1.5406 Å), and the intensities were recorded in a 2θ range from 10 to 90 degrees. Nitrogen adsorption measurement at 77 K was used to characterize the specific surface area of beads, pore volume, and pore size. The Brunauer-Emmett-Teller (BET) technique was employed to analyze the nitrogen adsorption isotherms and calculate the surface area and porosity of the beads. A Micromeritics Tristar 3000 coupled analyzer (Tokyo, Japan) was used for the analysis.

Packed Bed Adsorption Experiment

The packed bed adsorption experiment was conducted in a glass cylindrical polystyrene column that measured 0.587 meters in depth and had an interior diameter of 0.0342 meters. The column was loaded with pre-activated GCCHI beads to achieve the height of 1.2 m. The investigation was carried out at room temperature, employing atomic absorption spectrometry to examine the Ni^{2+} and Cd^{2+} ions in the aqueous mixture before and after adsorption, explicitly using a Varian SpectrAA-10 for this analysis. 85 grams of GCCHI were used for this experiment. During the experiment, the solution pH was kept constant (7 for Ni^{2+} and 6 for Cd^{2+}). Using pH 7 for Ni^{2+} offers the optimal deprotonation of chitosan

amino groups for optimum metal binding without nickel hydroxide precipitation. For Cd^{2+}, the optimal pH is 6 to ensure sufficient accessibility of the amines while avoiding premature cadmium hydrolysis. Both values ensure optimal efficiency in adsorption and ensure metal ion solubility. They are also conditions identified by earlier experimental work that are optimal [6]. The selection of pH ensures a realistic representation by the Swan model for packed bed columns.
The experimental setup allowed for the precise measurement of the concentration of Ni^{2+} and Cd^{2+} ions before and after the adsorption process. This was essential for determining the adsorption efficiency and capacity of the GCCHI beads. The use of atomic absorption spectrometry provided a reliable method for quantifying the metal ions, as it is well-established in the literature for its accuracy and sensitivity in detecting trace metals in various matrices [7].

Isotherm experiment

Isotherm tests placed 4 g of GCCHI beads into 250 mL Erlenmeyer flasks, each filled with 100 mL of nickel and cadmium solution at an initial 40 mg/L concentration. The initial concentration was made from a stock solution and then adjusted to the optimal pH. The Erlenmeyer flasks were placed in a labcon incubator for 50 minutes at an agitation speed of 120 rpm to achieve equilibrium. Isotherms were carried out at room temperature. Following equilibrium, a transparent metal solution was collected and examined using an atomic absorption spectrophotometer (Varian SpectrAA-10) obtained from Tokyo, Japan, to determine the amount of metal ions adsorbed. The equilibrium adsorption capacity was calculated from the mass balance equation as shown in Eq.1.

$$q_e = \frac{(C_0 - C_e)xV}{M} \tag{1}$$

Where q_e(mg/g) is the equilibrium adsorption capacity, C_o and C_e are the initial and equilibrium concentration (mg/L) of heavy metal ion in solution, respectively. At the same time, V (mL) is the volume and M (g) is the weight of the adsorbent.

Kinetic experiment

4 g of GCCHI beads were combined with 100 mL of metal ion solution in a 250 mL Erlenmeyer flask with 40 mg/L starting concentrations. The initial concentration was derived from a stock solution and then adjusted to the desired pH. To achieve equilibrium, the Erlenmeyer flasks were put in a labcon incubator, and the solutions were shaken at 120 rpm at room temperature. Samples were obtained at intervals of 30 minutes, 60 minutes, 90 minutes, 120 minutes, and 150 minutes and evaluated for metal ion removal using an atomic absorption spectrophotometer.

Langmuir and Freundlich Models for Adsorbent Binding Capacity

Adsorption isotherms are essential for evaluating how the adsorption process functions, particularly in determining the binding capacity of adsorbents. Two widely used models, the Langmuir and the Freundlich isotherms, are often applied for this purpose. The Langmuir model assumes monolayer adsorption, meaning that adsorption occurs at specific homogeneous sites on the adsorbent surface, leading to single-layer adsorption. This behavior is mathematically represented by the linear form of the Langmuir isotherm, shown in Eq. 2 [8].

$$\frac{C_e}{q_e} = \frac{C_e}{Q_m} + \frac{1}{Q_m K_L} \quad \text{(Linear form)} \tag{2}$$

The Langmuir constant Q_m (mol/g) represents the maximal adsorption capacity, while the bonding energy of adsorption is shown by K_L (L/mol). The K_L shows how to affirm that the adsorbate ions are bound to GCCHI beads. Greater K_L values denote substantially enhanced metal ion binding affinities. The slope and intercept of Ce/q_e vs C_e might be used to determine the parameters of the Langmuir model. The separation factor (R_L), which was employed to assess whether an adsorption system is favorable or unfavorable, as given in Eq. 3, can be used to represent the fundamental properties of the Langmuir model. RL greater than 1, RL = 1, and RL between 0 and 1 denote unfavorable, linear, and favorable circumstances.

$$R_L = \frac{1}{1+K_L C_O} \quad (3)$$

Considering how diverse surfaces interact in equilibrium, the Freundlich isotherm was developed. The isotherm originates from the notion that the distribution of adsorption sites is connected substantially to the degree of adsorption. It also suggests that the higher the adsorption sites, the quicker they saturate [9] Eq. 4 gives this model's linear description.

$$\log q_e = \log K_F + \frac{1}{n}\log C_e \quad (4)$$

The constants K_F and n correspondingly signify the adsorption intensity and capacity. The adsorbent's likelihood of being classified as more reactive increases with increasing K_L values [10,11] The slope and intercepts of the $\log q_e$ against the $\log C_e$ plot can be used to determine the parameters of this model. The range of n values should be between 1 and 10.

Influence of Kinetic Models

The process dynamics play a critical role in determining the residence time of adsorbate ions, with kinetic models frequently employed to explore these effects. Among the most widely used are the pseudo-first-order kinetics, introduced by Lagergren, and the pseudo-second-order kinetic model, as represented in Eqs. 5 and 6. These models are essential for analyzing the mechanisms that control adsorption processes, offering insights into the underlying factors regulating ion interactions and system efficiency.

$$\log(q_e - q_t) = \log(q_e) - t\frac{k_1}{2.303} \quad (5)$$

Correspondingly, qe and qt represent the proportion of metal ions absorbed on the adsorbent (mmol/g) at equilibrium and time t. The pseudo-first-order kinetics' rate constant is k_1 (min^{-1}). The straight-line plot of $\log(q_e - q_t)$ versus t Allows for the determination of the rate constant.

$$\frac{t}{q_t} = \frac{1}{K_2 q^2_e} + \frac{1}{q_e}t \quad (6)$$

Where k_2 (g/mmol.min) is the rate constant for a pseudo-second-order model, and q_e and q_t have the same definitions. Eq. 6 slope and intercept of the fitted line of t/qt vs. t determines the values of q_e and k_2.

Evaluation of Model Accuracy through Error Analysis

The effectiveness of the pseudo-first-order and pseudo-second-order kinetic models was evaluated by applying Marquardt's percent standard deviation (MPSD) test, as illustrated in Eq. 7. This non-linear statistical method compares experimental data against predicted data concerning the equilibrium adsorption capacity q_e.

$$MPSD = 100\sqrt{\frac{1}{N-P}\sum_{i=1}^{n}\left(\frac{\left(q_{e(\exp)} - q_{e(pred)}\right)^2}{q_{e(\exp)}}\right)i} \quad (7)$$

where N is the number of measurements, P is the number of parameters in the model, $q_{e(exp)}$ and $q_{e(pred)}$ are experimental and predicted uptake rates, respectively.

Column Regeneration

Desorption investigations commenced when the outlet concentrations of Ni^{2+} and Cd^{2+} ions were close to the inlet concentrations. The spent GCCHI beads underwent several washes in 2 L of purified water before desorption. Subsequently, the column was vacuum dried to ensure complete surface drying before desorption with 0.1 M HCl at a 5 mL/min rate. After the regeneration procedure, the

GCCHI beads were rinsed with purified water to remove excess acid. The vacuum drying method utilized in this study ensured that the GCCHI beads were adequately dried, which is crucial for the subsequent desorption phase.

Application of the Shrinking Core Model to Adsorption Kinetics

The shrinking core model was utilized to elucidate the kinetics of adsorption processes. The emphasis on the model is described in the work of [12]. This model posits that the adsorbate is confined within an active core. This suggests that intraparticle dispersion through the adsorbate-filled shell is the primary resistance to mass transfer during the uptake process. This phenomenon adheres to the distribution equation presented in Eq. 8.

$$\frac{\partial q}{\partial t} = \frac{k_L a \frac{3D_{eff}}{R_S^2 \rho \left(\frac{1-(1-\theta)^{1/3}}{(1-\theta)^{1/3}} \right)}}{k_L a + \frac{3D_{eff}}{R_S^2 \rho \left(\frac{1-(1-\theta)^{1/3}}{(1-\theta)^{1/3}} \right)}} C_B \quad (8)$$

However, various studies have employed empirical correlations to estimate the mass transfer coefficient, as demonstrated in [13,14]. The semi-empirical relationship outlined in Eq. 9 was utilized to facilitate this estimation.

$$Sh = 2.0 + 0.60 Re^{1/2} Sc^{1/3} \quad (9)$$

In which the Reynolds number, Re, has no dimensions, $\frac{d_p v \rho}{\mu}$The Schmidt number, Sc, has no dimensions. $\frac{\mu}{D_w \rho}$ And the Sherwood number, Sh, has no dimensions, $\frac{K_L d_p}{D_W}$

where D_{eff} is the efficient dispersion coefficient (m^2/s), C_B is the bulk mixture ion concentration (mol/L), R is the radius of the bead (m), ρ It is the metal ion density (kg/m^3) and the fraction filled capacity.

$$\theta = {q(t)}/{q_e} \quad (10)$$

The ratio of metal loading to total capacity varies from the initiation of binding until equilibrium is reached. This ratio, denoted as (θ), is represented in Eq. 10. Furthermore, the effective dispersion coefficient can be determined by fitting it to Eq. 8, utilizing equilibrium values obtained from the experimental assessment of time-dependent binding alongside the achieved q_e value.

Results and Discussion

XRD analysis of CHI, CCHI, and GCCHI Beads

X-ray diffraction (XRD) was carried out on a Bruker D8 Advance diffractometer (Germany) using a Cu Kα radiation source (λ = 1.5406 Å, anticathode: copper). The diffractometer was operated at 40 kV and 40 mA using a 10° to 90° 2θ scan range with a step size of 0.02° and a scan rate of 2°/min. XRD analysis of CHI, CCHI, and GCCHI beads revealed distinct peak patterns influencing their adsorption performance. The CHI beads exhibited a characteristic peak at 2θ = 20° (110 planes), consistent with the literature [15], indicating a densely packed structure that may limit functional group accessibility. In contrast, CCHI beads retained this peak but required cross-linking for acidic stability. GCCHI beads showed a shifted peak at 2θ = 23° with reduced intensity, signaling lower crystallinity due to disrupted hydrogen bonds from grafting. This structural loosening enhanced Ni^{2+}/Cd^{2+} adsorption by exposing more NH_2/OH groups. The amorphous nature of GCCHI, evidenced by broader peaks and loss of the 10° peak, correlated with higher surface area availability [15]. Aligning with its superior adsorption capacity. These findings underscore the crystallinity-adsorption

trade-off: ordered structures hinder metal ion access but improve robustness, while amorphous domains optimize binding sites at the expense of durability. The Swan model effectively linked these structural changes to dynamic adsorption behavior, supporting tailored material design for water treatment applications.

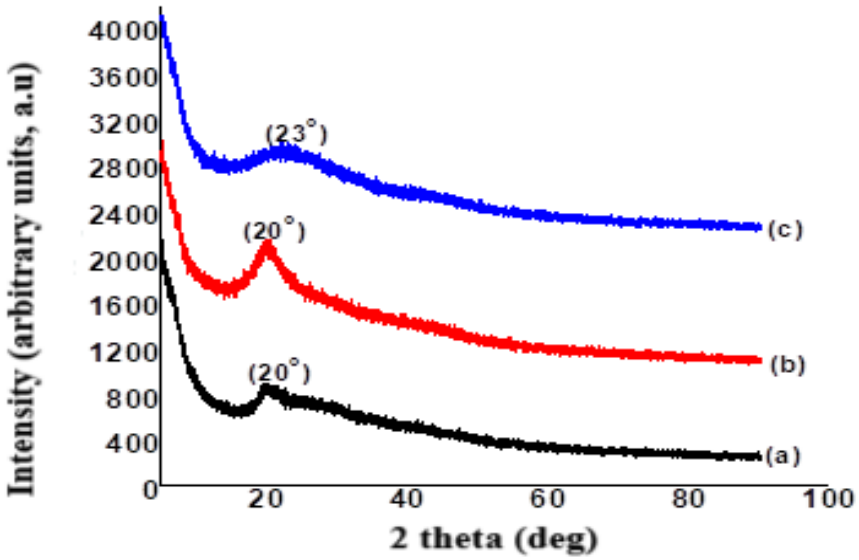

Fig. 1. XRD pattern of (a) CHI, (b) CCHI, and (c) GCCHI beads, respectively.

Surface Area and Porosity Characterization of Chitosan Beads Using BET and BJH Techniques.

The nitrogen adsorption-desorption isotherms in Figures 2a and 2b were applied to assess surface area and the pore size distribution on CHI, CCHI, and GCCHI using the BET and BJH methods. Significant variations in the isotherms are due to the mesoporous structure of the beads. The GCCHI bead sample shows the type IV isotherm characterized by a large hysteresis loop and high relative pressure factor. In contrast, CHI and CCHI bead samples show typical adsorption behavior. Quantitative studies show that the surface area and pore volume of the GCCHI beads are observably greater than those of CHI and CCHI samples.

The pore volume of the CHI, CCHI, and GCCHI beads is 0.633, 0.468, and 0.937 cm^3/g, respectively, while the surface area is 270.44, 250.32, and 302.12 m^2/g, respectively. The increase in BET surface area and pore volume for the GCCHI beads is mainly because of the development of new pores, a process caused by introducing additional amine groups as pillars into the bead matrix. Such increased porosity and surface area of the GCCHI beads enable greater efficiency in adsorption and desorption processes of pollutants, thereby increasing their potential in environmental remediation applications. Such findings have also been reported in other research [16]. Highlighting the significance of structural modification in improving biopolymer materials' adsorption capacity.

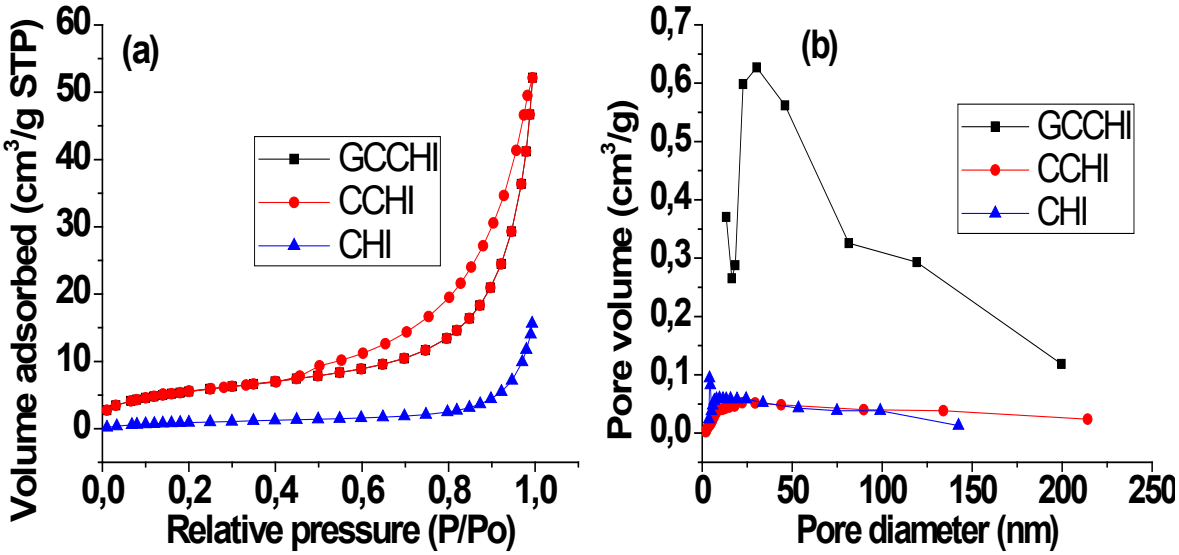

Fig. 2. Nitrogen adsorption/desorption isotherms at 77K for GCCHI beads, (a) BET, (b) BJH technique.

Evaluation of Breakthrough Curves for Ni^{2+} and Cd^{2+} Adsorption in a Column System

The breakthrough profiles for the adsorption of metal ions were evaluated under a controlled experimental setup characterized by a bed height of 1.20 m, a constant flow rate of 5.0 mL/min, and an inlet concentration of 30 mg/L [14]. The input parameters utilized in the column model are detailed in Table 1.

Table 1. Variables applied in predicting experimental data.

Variables	Amount
Weight of wet beads (g)	85
Average adsorbent size (mm)	1.3
Density ρ (kg/m³)	1100
Surface area per unit weight, α m^2/kg	88.7
The pH of the mixture of cadmium	6.0
The pH of the mixture of nickel	7.0
Equilibrium constant	$2.5x10^{-3}$
GCCHI beads capacity (mmol/g)	5.2
n and m	1.0
Adsorbate's molecular diffusion coefficient in water (m^2/s)	$2.0.\ 10^{-9}$
Adsorbate's external mass transfer coefficient, k (m/s)	$3.92.\ 10^{-6}$

Figures 3a and 3b present the breakthrough curves for Ni^{2+} and Cd^{2+} ions, respectively. A particle model was formulated to represent the experimental breakthrough curves, as shown in Eq. 8. The Swan model was employed due to its superior predictive capabilities regarding the experimental breakthrough curves, mainly by incorporating pH equilibrium values. The pH model is instrumental in calculating equilibrium results, which subsequently allows for determining the maximum adsorption capacity (q_{max}) and the equilibrium constant (K_{ads}) from the equilibrium data.

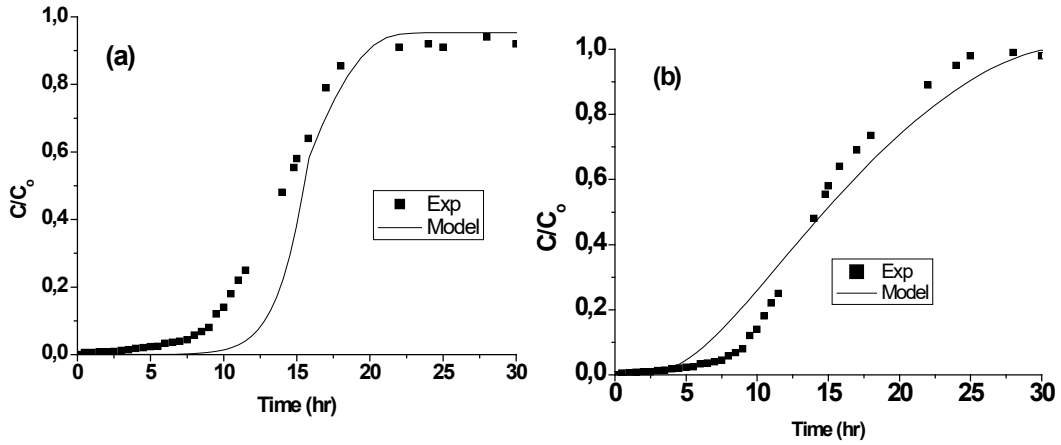

Fig. 3. Breakthrough curves for the adsorption of (a) Ni^{2+} and (b) Cd^{2+} ions onto GCCHI beads, with a flow rate of 5.0 mL/min, influent concentration of 30 mg/L, and temperature of 45°C.

The external mass transfer coefficient, a critical parameter in the modeling process, was derived through an empirical relationship between the Reynolds and Schmidt numbers, as articulated in Eq. 9. The diffusion coefficients were iteratively adjusted to achieve a satisfactory fit between the model and the experimental data. The diffusion coefficients were established at 3.14×10^{11} m^2/s for Cd^{2+} ions and 3.65×10^{11} m^2/s for Ni^{2+} ions. The agreement between the model predictions and experimental breakthrough curves confirms the model's credibility for predicting adsorption processes.

Kinetic Parameter Analysis of Metal Ion Adsorption onto GCCHI Beads

The kinetic parameters for the batch mode adsorption of metal ions onto GCCHI beads are summarized in Table 2. The data indicate a clear preference for the pseudo-second-order kinetic model over the pseudo-first-order model in describing the adsorption of Ni^{2+} and Cd^{2+} ions. Specifically, the correlation coefficients (R^2) for the pseudo-second-order model are significantly higher, approaching unity, which suggests a better fit to the experimental data than the pseudo-first-order model. The experimental qe values were 1.89 and 1.54 mmol/g for Cd^{2+} and Ni^{2+} ions, respectively. This observation aligns with findings from previous studies that emphasize the effectiveness of the pseudo-second-order model in capturing the kinetics of metal ion adsorption, indicating that the adsorption process is likely governed by chemisorption mechanisms involving interactions between the adsorbent's functional groups and the metal ions [17]. The Mean percentage standard deviation (MPSD) values further corroborate these findings, with lower MPSD values for the pseudo-second-order model indicating a strong agreement between experimental and predicted data. Conversely, the higher MPSD values associated with the pseudo-first-order model reflect a poor fit, reinforcing the conclusion that the pseudo-second-order model is more suitable for these adsorption processes [18]

Table 2. Kinetic variables for the adsorbate binding onto GCCHI beads at pH NI^{2+} (7) and Cd^{2+} (6), 120 RPM of agitation, and 70 min of contact.

Metal ions	Pseudo-first-order parameters				Pseudo-second-order parameters			
	k_1 (min^{-1})	$q_{e(pred)}$ (mmol/g)	MPSD	R^2	k_2 (g/mmol.min)	$q_{e(pred)}$ (mmol/g)	MPSD	R^2
Ni^{2+}	0.04	2.21	9.34	0.78	7.44	1.55	0.45	0.97
Cd^{2+}	0.01	1.87	10.65	0.73	7.14	1.86	1.11	0.97

Isotherm result

The correlation coefficient (R^2) was assessed to measure the effectiveness of the used models. Table 3 lists the isotherm model variables for adsorbate binding onto GCCHI at room temperature. R^2 readings for the adsorption of Ni^{2+} and Cd^{2+} ions onto GCCHI beads suggest that the results are well characterized by the Langmuir model (≥0.98), as opposed to the Freundlich model R^2 value (≥0.71). The maximum adsorption capacity (Q_{max}) obtained from the Langmuir model was 220 and 226 mg/g for Ni^{2+} and Cd^{2+} ions, respectively. The 'R_L' values for the Ni^{2+} and Cd^{2+} ions were 0 and 0.38, respectively. These values indicate a better adsorption mechanism [19].

Table 3. Binding of metal ions onto GCCHI beads at room temperature analyzed according to the Langmuir and the Freundlich isotherm models.

	Langmuir parameters			Freundlich parameters		
Pollutants	Q_{max} (mg/g)	R_L (L/mg)	R^2	n	K_f (mg/g)	R^2
Ni^{2+}	220	0.66	0.99	4.45	14.87	0.74
Cd^{2+}	226	0.37	0.99	4.32	14.11	0.72

Q_{MAX} Comparison

The maximum adsorption capacity obtained in this study was compared with that in the literature for the adsorption of Ni^{2+} and Cd^{2+} ions on various adsorbents (Table 3). It can be shown that GCCHI beads are highly effective for removing metal ions.

Table 3. Adsorption capacity comparison with other adsorbents.

Adsorbent	Target Metal	Max Adsorption Capacity (mg/g)	Reference
GCCHI beads (hypothetical)	Ni^{2+}	220	This study
	Cd^{2+}	226	This study
Fe_3O_4-ZrO_2@APS nanocomposite	Ni^{2+}	128	[20]
	Cd^{2+}	113	[20]
Zeolite	Cd^{2+}	48.63	[21]
Activated carbon	Ni^{2+}	100	[22]
Montmorillonite (Fe-modified)	Cd^{2+}	5.86	[23]

Regeneration and Recovery of Metal Ions from Utilized GCCHI Adsorbents

The rapid elution of Ni^{2+} and Cd^{2+} from GCCHI beads achieves remarkable concentration enrichment, desorbing ions from an initial 30 mg/L to over 2500 mg/L (Table 4). This process occurs as protons displace metal ions from binding sites, with the beads' porous structure facilitating migration into

solution. Internal diffusion emerges as the rate-limiting step, while decreasing recovery efficiency across cycles reflects active site saturation and potential complex formation. pH-dependent surface charge and metal speciation further influence desorption effectiveness, consistent with established adsorption principles.

Table 4. Removal efficiency of Ni^{2+} and Cd^{2+} ions at each stage of desorption

Degradation circle	Removal efficiency for Ni^{2+} ions	Removal efficiency for Cd^{2+} ions
1st circle	98.21	96.78
2nd circle	98.33	96.98
3rd circle	98.48	96.95
4th circle	98.45	96.92
5th circle	98.22	96.56

Desorption of Ni^{2+} and Cd^{2+} ions occurred rapidly within the first 30 minutes (Figure 4), followed by a gradual decline in concentration, indicating varying rates throughout the process. The results align with studies using 1 M HCl for efficient adsorbent regeneration [3], confirming its effectiveness for heavy metal recovery. These findings underscore the importance of modeling desorption kinetics to optimize adsorption-desorption cycles.

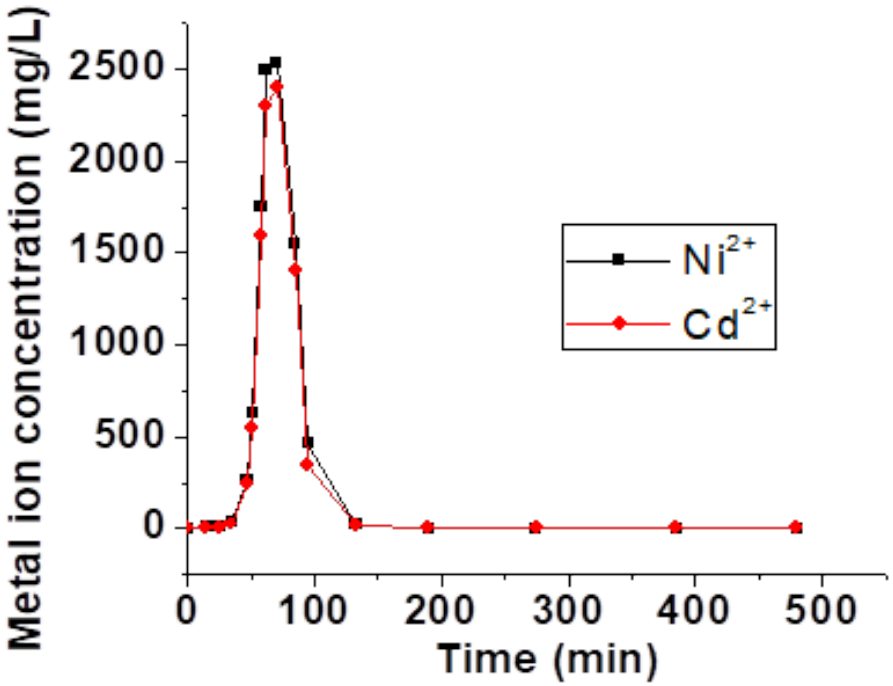

Fig. 4. Regeneration curves for Ni^{2+} and Cd^{2+} ions employing a 5.0 mL/min flow rate of 0.1 M HCl mixture.

Durability and Efficiency of GCCHI Beads in Adsorption-Desorption Cycles

Five consecutive adsorption-desorption cycles demonstrated the reusability of GCCHI beads, with breakthrough curves revealing consistent performance (Figure 5). While the beads maintained stable mass retention and adsorption capacity in the first cycle, subsequent cycles showed a gradual mass loss (0.4–1.6%) and a slight improvement in removal efficiency from cycles 2 to 4, likely due to acid-induced pore opening and improved bead uniformity. However, long-term durability remains challenging, as declining adsorption efficiency and structural stability were observed in later cycles.

Despite this, GCCHI beads outperformed many chitosan-based adsorbents in the literature [24,25] highlighting their potential for practical applications with further optimization. Most research indicates chitosan derivatives lose 10–30% capacity after five cycles [26,27]. The developed adsorbent maintains more than 95% efficiency for Ni^{2+} and Cd^{2+} even after several regenerations. The finding indicates that GCCHI beads perform better than pure chitosan and compete with modified composites in reusability. The future development of GCCHI beads for widespread adsorption requires either matrix changes to chitosan materials or protective chemical implementation to enhance operational stability.

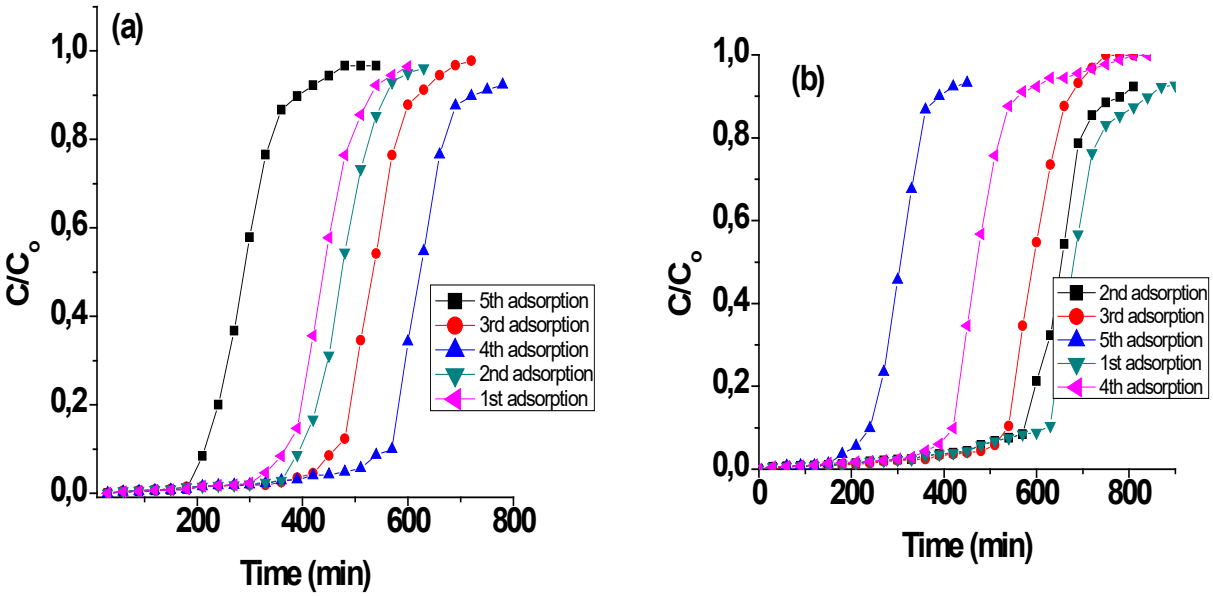

Fig. 5. Breakthrough curve for the five cycles of (a) Ni^{2+} and (b) Cd^{2+} ions adsorption onto GCCHI beads.

Mechanisms and Real-world Relevance

The Ni^{2+} and Cd^{2+} adsorption on GCCHI beads is chelation-induced via metal ion-functional group interactions of chitosan and pH-dependent electrostatic interactions. Kinetic changes are observed upon breakthrough curves in which Cd^{2+} is typically marked by delayed breakthrough compared to $Ni^{2,+}$ since Cd^{2+} is a softer Lewis acid with a higher binding affinity. The shape of the curves shows the adsorption kinetics, whereby steeper slopes indicate higher kinetics governed by pore diffusion and less steep slopes indicate surface diffusion control. As far as applications are concerned, the adsorption capacity and regenerability of the GCCHI beads position them to be applied for industrial wastewater treatment, particularly in metal plating and mining industries, where heavy metal pollution is prevalent. The ability to reuse and regenerate the beads on multiple occasions without any loss in performance presents an economic option over conventional treatment techniques. Also, the soundness of applying the Swan model to simulate breakthrough behavior makes it possible for water treatment systems to be designed on a scale that will fulfill environmental standards for heavy metal discharge. This approach not only overcomes the technical issues in water purification but is also a sustainable practice that employs a biodegradable adsorption material. This work illustrates that combining material science with process engineering is a significant step towards practical, efficient, and green technology for removing heavy metals.

Conclusion

The study proved the efficiency of chitosan derivatives, specifically GCCHI, in adsorbing Cd^{2+} and Ni^{2+} ions from aqueous solution. The adsorption performance of the GCCHI bead depends solely on working conditions, including pH. The highest removal efficiencies of Cd^{2+} and Ni^{2+} were achieved at pH 6 and 7, respectively. Notable alterations were made to CHI beads, which resulted in increased surface areas, large pore volumes, and greater amounts of active sites. The modification method applied to CHI increased its adsorption capacity, making it the best candidate for environmental remediation compared to other chitosan derivatives. The removal efficiency remained the same during this study after repeated regeneration cycles. Research must prioritize the actual wastewater use of GCCHI in upcoming investigations.

Acknowledgments

The author wishes to thank the Durban University of Technology's Department of Chemical Engineering for providing continuous working facilities.

References

[1] J. Kabuba, A.V. Maliehe, Application of neural network techniques to predict the heavy metals in acid mine drainage from South African mines, Water Science and Technology 84 (2021) 3489–3507. https://doi.org/10.2166/wst.2021.494.

[2] N.A.A. Qasem, R.H. Mohammed, D.U. Lawal, Removal of heavy metal ions from wastewater: a comprehensive and critical review, NPJ Clean Water 4 (2021). https://doi.org/10.1038/S41545-021-00127-0.

[3] S. Bin Kang, Z. Wang, S.W. Won, Evaluation of Adsorption and Desorption Properties of PAAPSBF for Cd(II) from Aqueous Solution, Chem Eng Trans 89 (2021) 259–264. https://doi.org/10.3303/CET2189044.

[4] Asma Ashraf, Joydeep Dutta, Aiman Farooq, Mohd. Rafatullah, Kaushik Pal, George Z. Kyzas, Chitosan-based materials for heavy metal adsorption: Recent advancements, challenges and limitations, J Mol Struct 1309 (2024).

[5] P.O. Osifo, The use of chitosan beads for the adsorption and regeneration of heavy metals, (2007) 156. https://repository.nwu.ac.za/bitstream/handle/10394/1635/osifo_petero.pdf?sequence=1&isAllowed=y.

[6] E. Igberase, P. Osifo, A. Ofomaja, The Adsorption of Pb, Zn, Cu, Ni, and Cd by Modified Ligand in a Single Component Aqueous Solution: Equilibrium, Kinetic, Thermodynamic, and Desorption Studies, Int J Anal Chem 2017 (2017). https://doi.org/10.1155/2017/6150209.

[7] S. Kim, S.N. Nam, A. Jang, M. Jang, C.M. Park, A. Son, N. Her, J. Heo, Y. Yoon, Review of adsorption–membrane hybrid systems for water and wastewater treatment, Chemosphere 286 (2022). https://doi.org/10.1016/j.chemosphere.2021.131916.

[8] D. A.O, Langmuir, Freundlich, Temkin and Dubinin–Radushkevich Isotherms Studies of Equilibrium Sorption of Zn 2+ Unto Phosphoric Acid Modified Rice Husk, IOSR Journal of Applied Chemistry 3 (2012) 38–45. https://doi.org/10.9790/5736-0313845.

[9] R. Bargagli, Moss and lichen biomonitoring of atmospheric mercury: A review, Science of the Total Environment 572 (2016) 216–231. https://doi.org/10.1016/j.scitotenv.2016.07.202.

[10] C. Dong, F. Zhang, Z. Pang, G. Yang, Efficient and selective adsorption of multi-metal ions using sulfonated cellulose as adsorbent, Carbohydr Polym 151 (2016) 230–236. https://doi.org/10.1016/j.carbpol.2016.05.066.

[11] L. Zhang, Y. Zeng, Z. Cheng, Removal of heavy metal ions using chitosan and modified chitosan: A review, J Mol Liq 214 (2016) 175–191. https://doi.org/10.1016/j.molliq.2015.12.013.

[12] M. Banza, H. Rutto, T. Seodigeng, Application of Artificial Neural Network and Shrinking Core Model for Copper (Ii) and Lead (Ii) Leaching from Contaminated Soil Using Ethylenediaminetetraacetic Acid, Soil Sediment Contam (2023). https://doi.org/10.1080/15320383.2023.2178384.

[13] P.O. Osifo, A. Webster, H. van der Merwe, H.W.J.P. Neomagus, M.A. van der Gun, D.M. Grant, The influence of the degree of cross-linking on the adsorption properties of chitosan beads, Bioresour Technol 99 (2008) 7377–7382. https://doi.org/10.1016/j.biortech.2008.01.053.

[14] E. Igberase, P.O. Osifo, Mathematical modelling and simulation of packed bed column for the efficient adsorption of Cu(II) ions using modified bio-polymeric material, J Environ Chem Eng 7 (2019). https://doi.org/10.1016/j.jece.2019.103129.

[15] H.E. Abdelwahab, M. Elhag, M.M. El Sadek, Removal of As(V) and Cr(VI) using quinoxaline chitosan schiff base: synthesis, characterization and adsorption mechanism, BMC Chem 18 (2024). https://doi.org/10.1186/s13065-024-01328-7.

[16] E. Igberase, P.O. Osifo, Application of diethylenetriamine grafted on glyoxal cross-linked chitosan composite for the effective removal of metal ions in batch system, Int J Biol Macromol 134 (2019). https://doi.org/10.1016/j.ijbiomac.2019.05.179.

[17] L.D. Pompeu, P.C.L. Muraro, G. Chuy, B.S. Vizzotto, G. Pavoski, D.C.R. Espinosa, L. da Silva Fernandes, W.L. da Silva, Adsorption for rhodamine b dye and biological activity of nano-porous chitosan from shrimp shells, Environmental Science and Pollution Research 29 (2022) 49858–49869. https://doi.org/10.1007/s11356-022-19259-y.

[18] N. Can, B.C. Ömür, A. Altındal, Modeling of heavy metal ion adsorption isotherms onto metallophthalocyanine film, Sens Actuators B Chem 237 (2016) 953–961. https://doi.org/10.1016/j.snb.2016.07.026.

[19] E. Igberase, A. Ofomaja, P.O. Osifo, Enhanced heavy metal ions adsorption by 4-aminobenzoic acid grafted on chitosan/epichlorohydrin composite: Kinetics, isotherms, thermodynamics and desorption studies, Int J Biol Macromol 123 (2019). https://doi.org/10.1016/j.ijbiomac.2018.11.082.

[20] C. Bulin, T. Guo, Ultra fast and highly efficient recovery of cadmium with graphene oxide-chitosan grafted by nickel ferrite as a recyclable adsorbent and atomic scale mechanism, Science of the Total Environment 991 (2025). https://doi.org/10.1016/j.scitotenv.2025.179974.

[21] H. Li, K. Han, J. Shang, W. Cai, M. Pan, D. Xu, C. Du, R. Zuo, Comparison of Adsorption Capacity and Removal Efficiency of Strontium by Six Typical Adsorption Materials, Sustainability (Switzerland) 14 (2022). https://doi.org/10.3390/su14137723.

[22] M.A. Kaczorowska, D. Bożejewicz, The Application of Chitosan-Based Adsorbents for the Removal of Hazardous Pollutants from Aqueous Solutions—A Review, Sustainability (Switzerland) 16 (2024). https://doi.org/10.3390/su16072615.

[23] H. Li, K. Han, J. Shang, W. Cai, M. Pan, D. Xu, C. Du, R. Zuo, Comparison of Adsorption Capacity and Removal Efficiency of Strontium by Six Typical Adsorption Materials, Sustainability (Switzerland) 14 (2022). https://doi.org/10.3390/su14137723.

[24] X. qi Liu, X. xin Zhao, Y. Liu, T. an Zhang, Review on preparation and adsorption properties of chitosan and chitosan composites, Polymer Bulletin 79 (2022) 2633–2665. https://doi.org/10.1007/s00289-021-03626-9.

[25] U. Haripriyan, K.P. Gopinath, J. Arun, Chitosan based nano adsorbents and its types for heavy metal removal: A mini review, Mater Lett 312 (2022). https://doi.org/10.1016/j.matlet.2022.131670.

[26] A. Singh, N. Singh, N. Kaur, D.O. Jang, Chitosan-poly(vinyl alcohol)-ionic liquid-grafted hydrogel for treating wastewater, New Journal of Chemistry 47 (2023) 11196–11209. https://doi.org/10.1039/D3NJ01384G.

[27] P.O. Osifo, A. Webster, H. van der Merwe, H.W.J.P. Neomagus, M.A. van der Gun, D.M. Grant, The influence of the degree of cross-linking on the adsorption properties of chitosan beads, Bioresour Technol 99 (2008) 7377–7382. https://doi.org/10.1016/J.BIORTECH.2008.01.053.